Inorganic Chemistry

Article

pubs.acs.org/IC

Synthesis, Crystal Structures, and Dual Donor Luminescence Sensitization in Novel Terbium Tetracyanoplatinates

Philip A. Smith,[‡] Carlos Crawford,[†] Nuquie Beedoe,[†] Zerihun Assefa,*[,†] and Richard E. Sykora*[,‡]

[†]Department of Chemistry, North Carolina A&T State University, Greensboro, North Carolina 27411, United States

[‡]Department of Chemistry, University of South Alabama, Mobile, Alabama 36688, United States

Supporting Information

ABSTRACT: A series of novel terbium tetracyanoplatinate compounds all incorporating tridentate 2,2′:6′2″-terpyridine (terpy) or 4′-chloro-2,2′:6′2″-terpyridine (terpy-Cl) were synthesized and used to investigate the phenomenon of dual-donor sensitization of Tb^{3+}. Judicious choice of the Tb^{3+} salt and reaction conditions results in the isolation of $\{Tb(terpy)(H_2O)_2(NO_3)Pt(CN)_4\}\cdot CH_3CN$ (**1A**), $\{Tb(terpy)(H_2O)_2(NO_3)Pt(CN)_4\}\cdot 3.5H_2O$ (**1B**), $\{Tb(terpy\text{-}Cl)(H_2O)_2(NO_3)Pt(CN)_4\}\cdot 2.5H_2O$ (**2**), $[Tb(terpy)(H_2O)_2(CH_3COO)_2]_2Pt(CN)_4\cdot 4H_2O$ (**3**), or $[Tb_2(terpy)_2(H_2O)_2(CH_3COO)_5]_2Pt(CN)_4\cdot 7H_2O$ (**4**). The compounds **1A**, **1B**, and **2** contain one-dimensional polymeric structures with bridging of $[Tb(L)(NO_3)(H_2O)_2]^{2+}$ (L = terpy or terpy-Cl) moieties by cis-bridging tetracyanoplatinate (TCP) anions as determined via single-crystal X-ray diffraction studies. Both **3** and **4**, however, contain Tb^{3+} coordinated by multiple acetate ligands and terpy, but not TCP, and are classified as zero-dimensional complex salts. Platinophilic interactions that dominate tetracyanoplatinate structural chemistry are present in the form of dimeric units in the polymeric compounds, but are totally absent in **3** and **4**. The structural differences result in markedly different luminescence properties for the two classes of compounds. All of the polymeric compounds display efficient donor−acceptor intramolecular energy transfer (IET) from the terpy unit to the Tb^{3+} ion. Although the TCP units are also directly coordinated to the Tb^{3+} ion in the three polymers, only in **1B** and **2** are the Pt···Pt interactions strong enough to provide MMLCT bands of appropriate energy to result in a dual-donor effect to the Tb^{3+} sensitization. Even in these cases, TCP does not efficiently sensitize the Tb^{3+}, rather a broad band TCP emission results. However, terpy and acetate ligands are bonded directly to the Tb^{3+} ion in **3** and **4** and provide a strong dual-donor sensitization effect as evidenced by the large QY for Tb^{3+}.

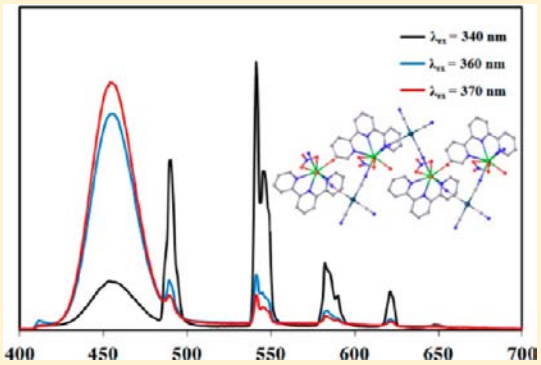

INTRODUCTION

Lanthanide ions are well-known for their characteristic sharp emissions in the visible and near-infrared (NIR) regions and long lifetimes which makes them attractive candidates for the development of optical devices including light-conversion materials.[1] Their unique optical and magnetic properties have promoted an increasing number of technological applications ranging from biomedical analysis (fluoroimmunoassays, MRI contrast agents, and cellular imaging) to materials science (lasers, optical fibers, light emitting diodes, optical displays, and electron luminescent devices).[2−11] Nevertheless the inherent inefficiency of the f-f electric dipole transitions (which are parity and potentially spin forbidden) and magnetic dipole transitions (which have oscillator strengths several orders of magnitude weaker than electric dipole transitions) remains a major obstacle that limits progress in application of these systems. In this regard, our interests lie in the production of novel lanthanide compounds containing multiple chromophoric ligands that photosensitize lanthanide-ion luminescence.

Donor ligands used for lanthanide emission sensitization usually have strong absorbance in the UV region and transfer their excited energy to the acceptor lanthanide ions.[12−14] A new class of chromophores involving transition metal complexes is emerging as suitable sensitizers of lanthanide ion acceptors,[15,16] in addition to the traditional organic ligands used for this purpose.[17] The tetracyanoplatinate anion is one such donor system that has been shown to meet these criteria.[18−24] A major advantage afforded by the former chromophores is their ability to sustain a better energy match-up with most Ln^{3+} acceptor states.[24−31] Additional unique advantages of metal complexes over organic chromophores are that they can provide a relatively high triplet quantum yield because of the rapid intersystem crossing inherent within the system (due to the heavy-atom effect) and the possibility of a facile detection of both quenching of the d-block chromophores and the sensitized emission from the lanthanide centers.[24−31]

Recent breakthroughs in low-dimensional nanostructures have led to a renewal of interest in polymers composed of platinum complexes.[32] As a result, the surge of research into one-dimensional platinum complexes in the 1960s through the 1980s[33−35] has given way to a steady progress of investigations

Received: June 28, 2012
Published: November 5, 2012

   dx.doi.org/10.1021/ic3013975 | *Inorg. Chem.* 2012, 51, 12230−12241

that have explored new ligands, and complexes with coordination polymeric features and examination of the influence of organic and inorganic cations and anions on the Pt···Pt distance and the overall structural features.[36−39]

In a similar vein, we have been studying coordination polymers built from tetracyano and dicyanometallates of the group 10 and 11 metals,[40−43] which act as donor species for various lanthanide ions.[15−17,25−30] Our goal is to explore a cooperative condition where multiple donor groups are able to pump the lanthanide ion and provide added strength in the sensitized emission. Studied systems have included (1) purely inorganic ligand systems such as in $K_2[Tb(H_2O)_4(Pt(CN)_4)_2]$-$Au(CN)_2 \cdot 2H_2O$[40] and (2) mixed ligand systems composed of both inorganic metal cyanide and traditional organic sensitizer ligands, for example, in $[Tb(C_{10}N_2H_8)(H_2O)_4(Pt(CN)_4)(Au(CN)_2)] \cdot 1.5C_{10}N_2H_8 \cdot 2H_2O$[40] ($C_{10}N_2H_8$ = 2,2′-bipyridine) and $Eu(C_{15}H_{11}N_3)(H_2O)_2(NO_3)(Pt(CN)_4) \cdot CH_3CN$.[41]

Particular advantages of the latter system[41] are the abilities to broaden the energy range for donor light harvesting and efficiently sensitize Eu^{3+} luminescence via energy transfer from the multiple donor groups. The recently reported findings in this area illustrated that syntheses of the materials by utilizing various counteranions could be used to modulate structural features. Correlation between the structural features and the energy transfer behavior was established, and therefore, the energy transfer behavior was modulated as a function of counteranion, and evidence for dual donor sensitization was thus illustrated. In this paper we will continue our investigation of dual-donor sensitization processes, where similar studies are reported on a number of terbium based compounds. The sensitization phenomenon is affected by the extent of donor−acceptor match-up and the energy transfer efficiencies. Herein, the sensitization processes of the Tb^{3+} acceptors will be presented and compared with those of Eu^{3+} in the related systems.[41]

EXPERIMENTAL SECTION

Materials and Methods. $Tb(NO_3)_3 \cdot xH_2O$ (Alfa Aesar, 99.9%), $Tb(CH_3COO)_3 \cdot xH_2O$ (Alfa Aesar, 99.9%), $K_2[Pt(CN)_4] \cdot 3H_2O$ (Alfa Aesar, 99.9%), 2,2′:6′,2″-terpyridine (Alfa Aesar, 99%), and 4′-chloro-2,2′:6′,2″-terpyridine (Alfa Aesar, 98%) were used as received without further purification. No attempts to carry out the reactions in dry conditions were made, and none of the nonaqueous solvents used in the syntheses were dried prior to use. IR spectra were obtained on neat crystalline samples at room temperature using a Jasco FT/IR-4100 with a diamond ATR attachment in the range 4000−650 cm^{-1} or on KBr discs using a Mattson Research Series (RS-10000) FTIR in the range 4000−400 cm^{-1}. CHN analyses were performed by Galbraith Laboratories, Inc. in Knoxville, TN.

Synthesis of $\{Tb(C_{15}H_{11}N_3)(H_2O)_2(NO_3)Pt(CN)_4\} \cdot CH_3CN$ (1A) and $\{Tb(C_{15}H_{11}N_3)(H_2O)_2(NO_3)Pt(CN)_4\} \cdot 3.5H_2O$ (1B). The syntheses of **1A** and **1B** have been conducted under the same reaction conditions as described below. First, 1 mL of 0.10 M $Tb(NO_3)_3$ and 1 mL of 0.10 M $K_2[Pt(CN)_4]$ are mixed. Next 1 mL of 0.10 M 2,2′:6′,2″-terpyridine was layered onto the former mixture. The $Tb(NO_3)_3$ and terpy solutions were prepared using CH_3CN as the solvent, while the $K_2[Pt(CN)_4]$ solution was made by dissolving $K_2[Pt(CN)_4] \cdot 3H_2O$ in a 20%:80% mixture of H_2O:CH_3CN. Slow evaporation of the solvent resulted in the crystallization of **1A** and/or **1B** as colorless single crystals. Multiple attempts have been made to determine subtle changes that lead to the preferential crystallization of **1A** vs **1B**, but these experiments have not been successful. We have noticed that the reaction products from a series of multiple, identical reactions are normally composed of only one of the products and not a mixture. Manual separation and identification of crystallites by unit cell determination was performed to ensure material purity for property measurements. Typical yields are 40−45%. IR(**1A**, solid, cm^{-1}): 653 (s), 743 (s), 774 (s), 815 (m), 922 (w), 973 (w), 1013 (s), 1038 (m), 1078 (w), 1162 (m), 1194 (w), 1235 (m), 1306 (s), 1370 (m), 1400 (m), 1482 (s), 1576 (m), 1599 (m), 1638 (m), 1665 (w), 2030 (m), 2138 (s), 2148 (s), 2181 (w), 3225 (m, br). IR(**1B**, KBr, cm^{-1}): 441 (s), 655 (s), 768 (s), 813 (m), 1014 (s), 1036 (m), 1075 (w), 1161 (m), 1167 (m), 1233 (m), 1302 (s), 1384 (m), 1396 (w), 1433 (s), 1451 (s), 1483 (s), 1573 (m), 1578 (m), 1601 (m), 2148 (s), 2164 (m), 2185 (w), 3200 (m, br), 3404 (m, br), 3603 (m). Elemental Analysis: **1A**, Calculated for $C_{21}H_{18}N_9O_5PtTb$: C, 30.4; H, 2.18; N, 15.18. Found: C, 19.44; H, 1.59; N, 12.98; **1B**, Calculated for $C_{19}H_{22}N_8O_{8.5}PtTb$: C, 26.77; H, 2.60; N, 13.14. Found: C, 23.54; H, 2.32; N, 13.14.

Synthesis of $\{Tb(C_{15}H_{10}ClN_3)(H_2O)_2(NO_3)Pt(CN)_4\} \cdot 2.5H_2O$ (2). The synthesis of **2** was conducted in EtOH by mixing the three following solutions: 1 mL of 0.10 M $Tb(NO_3)_3$, 1 mL of 0.1 M 4′-chloro-2,2′:6′,2″-terpyridine, and 1 mL of 0.20 M $K_2[Pt(CN)_4]$. The solution of 4′-chloro-2,2′:6′,2″-terpyridine required gentle heat for complete dissolution. Slow evaporation of the solvent resulted in the crystallization of **2** as colorless single crystals with a yield of 35%. IR(KBr, cm^{-1}): 413 (w), 425 (m), 433 (s), 572 (s), 637 (m), 657 (m), 680 (w), 729 (s), 742 (m), 788 (s), 814 (m), 870 (m), 1014 (s), 1036 (m), 1056 (w), 1063 (w), 1132 (m), 1235 (m), 1265 (w), 1300 (s), 1310 (s), 1340 (w), 1395 (m), 1412 (s), 1467 (s), 1483 (m,sh), 1554 (s), 1574 (m), 1590 (s), 1600 (,), 2146 (s), 2182 (w), 2854 (w), 2922 (w), 3212 (s, br), 3408 (s, br), 3508 (w), 3628 (w). Elemental Analysis: Calculated for $C_{19}H_{19}ClN_8O_{7.5}PtTb$: C, 26.26; H, 2.20; N, 12.90. Found: C, 24.49; H, 2.17; N, 12.84.

Synthesis of $[Tb(C_{15}H_{11}N_3)(H_2O)_2(CH_3COO)_2]_2Pt(CN)_4 \cdot 4H_2O$ (3). Compound **3** was synthesized by first mixing 1 mL of 0.10 M $Tb(CH_3COO)_3$ and 1 mL of 0.025 M $K_2[Pt(CN)_4]$. Next, a 1 mL solution of 0.10 M terpy was layered onto the mixture. The $Tb(CH_3COO)_3$ and $K_2[Pt(CN)_4]$ solutions were prepared using H_2O as the solvent, while the terpy solution was made by using acetonitrile as the solvent. Slow evaporation of the solvent resulted in the crystallization of **3** as colorless single crystals with a yield of 95%. IR(solid, cm^{-1}): 653 (s), 676 (s), 742 (w), 770 (s), 776 (s), 828 (w), 938 (m), 1013 (s), 1050 (w),1160 (m), 1201 (w), 1234 (m), 1307 (m), 1436 (s), 1450 (s), 1483 (m), 1528 (s), 1575 (w), 1600 (m), 1675 (m), 2137 (s), 3220 (m, br). Elemental Analysis: Calculated for $C_{42}H_{50}N_{10}O_{16}PtTb_2$: C, 34.46; H, 3.44; N, 9.57. Found: C, 31.35; H, 3.47; N, 7.84.

Synthesis of $[Tb_2(C_{15}H_{11}N_3)_2(H_2O)_2(CH_3COO)_5]_2Pt(CN)_4 \cdot 7H_2O$ (4). Compound **4** was synthesized by first mixing 1 mL of 0.10 M $Tb(CH_3COO)_3$ and 1 mL of 0.10 M $K_2[Pt(CN)_4]$. Next, a 1 mL solution of 0.10 M terpy was layered onto the mixture. The $Tb(CH_3COO)_3$ and $K_2[Pt(CN)_4]$ solutions were prepared using H_2O as the solvent, while the terpy solution was made by using acetonitrile as the solvent. Slow evaporation of the solvent resulted in the crystallization of **4** as colorless single crystals with a yield of 22%. IR(solid, cm^{-1}): 654 (s), 668 (s), 678 (s), 768 (m), 938 (w), 1013 (s), 1050 (w), 1160 (m), 1202 (m), 1234 (m), 1307 (m), 1405 (m), 1436 (s), 1451 (s), 1539 (s), 2135 (w), 3300 (m, br). Elemental Analysis: Calculated for $C_{84}H_{96}N_{16}O_{31}PtTb_4$: C, 37.98; H, 3.64; N, 8.44. Found: C, 33.21; H, 3.44; N, 9.03.

Single-Crystal X-ray Diffraction. Single crystals of all compounds were selected, mounted on quartz fibers, and aligned with a digital camera on a Varian Oxford Xcalibur E single-crystal X-ray diffractometer. Intensity measurements were performed using Mo Kα radiation, from a sealed-tube Enhance X-ray source, and an Eos area detector. CrysAlisPro[44] was used for preliminary determination of the cell constants, data collection strategy, and for data collection control. Following data collection, CrysAlisPro was also used to integrate the reflection intensities, apply an absorption correction to the data, and perform a global cell refinement.

All crystals examined in these studies diffracted extremely well and were not problematic in regards to structure solution and refinement. The program suite SHELX was used for structure solution (XS) and least-squares refinement (XL).[45] The initial structure solutions were carried out using direct methods, and the remaining heavy atom

dx.doi.org/10.1021/ic3013975 | Inorg. Chem. 2012, 51, 12230−12241

Table 1. Crystallographic Data for $Tb(C_{15}H_{11}N_3)(H_2O)_2(NO_3)Pt(CN)_4 \cdot CH_3CN$ (1A), $Tb(C_{15}H_{11}N_3)(H_2O)_2(NO_3)(Pt(CN)_4) \cdot 3.5H_2O$ (1B), $Tb(C_{15}H_{10}ClN_3)(H_2O)_2(NO_3)[Pt(CN)_4] \cdot 2.5H_2O$ (2), $[Tb(C_{15}H_{11}N_3)(H_2O)_2(CH_3COO)_2]_2Pt(CN)_4 \cdot 4H_2O$ (3), and $[Tb_2(C_{15}H_{11}N_3)_2(H_2O)_2(CH_3COO)_5]_2Pt(CN)_4 \cdot 7H_2O$ (4)

abbreviation	1A	1B	2	3	4
chemical formula	$C_{21}H_{18}N_9O_5PtTb$	$C_{19}H_{22}N_8O_{8.5}PtTb$	$C_{19}H_{19}ClN_8O_{7.5}PtTb$	$C_{42}H_{50}N_{10}O_{16}PtTb_2$	$C_{84}H_{96}N_{16}O_{31}PtTb_4$
formula weight (amu)	830.45	852.46	868.88	1463.85	2656.54
space group	$P2_1/c$ (No. 14)	*Pbcn* (No. 60)	*Pbcn* (No. 60)	$P\bar{1}$ (No. 2)	$P\bar{1}$ (No. 2)
a (Å)	12.8660(2)	13.3306(2)	13.3631(3)	12.0947(2)	12.2032(2)
b (Å)	15.1682(2)	15.9508(2)	16.0393(2)	12.7430(3)	12.6534(2)
c (Å)	13.6899(2)	24.4272(4)	24.0360(5)	18.6790(3)	18.2778(3)
α (deg)	90	90	90	92.848(2)	110.107(2)
β (deg)	105.550(2)	90	90	92.169(2)	90.7590(10)
γ (deg)	90	90	90	118.076(2)	112.6950(10)
V (Å^3)	2573.85(6)	5194.05(13)	5151.75(17)	2530.82(10)	2410.17(7)
Z	4	8	8	2	1
T (K)	290	290	290	290	290
λ (Å)	0.71073	0.71073	0.71073	0.71073	0.71073
ρ_{calcd} (g cm^{-3})	2.143	2.180	2.241	1.921	1.830
μ(Mo $K\alpha$) (mm^{-1})	8.204	8.142	8.309	5.597	4.429
$R(F_o)$ for $F_o^2 > 2\sigma(F_o^2)^a$	0.0159	0.0211	0.0229	0.0165	0.0243
$R_w(F_o^2)^b$	0.0295	0.0442	0.0591	0.0387	0.0481

$^a R(F_o) = \sum||F_o| - |F_c||/\sum|F_o|$. $^b R_w(F_o^2 = [\sum[w(F_o^2 - F_c^2)^2])/\sum wF_o^4]^{1/2}$.

positions were located in difference maps. The final refinements included anisotropic displacement parameters for all non-hydrogen atoms and isotropic refinements for the H positions. Refinement was performed against F^2 by weighted full-matrix least-squares and semiempirical absorption corrections were applied. Some crystallographic details are included in Table 1 and additional crystallographic details are available as Supporting Information. Data can also be obtained free of charge in cif format by request from The Cambridge Crystallographic Data Centre at www.ccdc.cam.ac.uk/data_request/cif with the CCDC numbers 873774, 873775, 873776, 873777, and 873778 for **1A**, **1B**, **2**, **3**, and **4**, respectively.

Photoluminescence Measurements. The luminescence spectra were collected using a Photon Technology International (PTI) spectrometer (model QM-7/SE). The system uses a high intensity Xe source for excitation. Selection of excitation and emission wavelengths are conducted by means of computer controlled, autocalibrated "QuadraScopic" monochromators and are equipped with aberration corrected emission and excitation optics. Signal detection is accomplished with a PMT detector (Hamamatsu model 928) that can work either in analog or digital (photon counting) modes. All of the emission spectra presented are corrected to compensate for wavelength dependent variation in the system on the emission channel. The emission correction files, which were generated by comparison of the emission channel response to the spectrum of a NIST traceable tungsten light, were used as received from PTI. The emission correction was conducted in real time using the PTI provided protocol. The instrument operation, data collection, and handling were all controlled using the advanced FeliX32 fluorescence spectroscopic package. The steady state emission and excitation spectra were collected upon continuous excitation (without introducing any time delay). For the time dependent measurements, various time delays were introduced ranging from 2 to 200 μs. Measurement of the Tb^{3+} lifetimes were conducted by exciting the samples with the N_2 laser line at 337.1 nm and monitoring the decay profile at the 541 nm emission. The TCP emission at ~450 nm was excited by pumping a dye emitting at 366.1 nm with a N_2 laser. All of the spectroscopic experiments were conducted on neat crystalline samples held in sealed quartz capillary tubes. The low temperature measurements were conducted on samples inserted in a coldfinger dewar filled with liquid nitrogen.

The absolute photoluminescence (PL) quantum yield (QY) measurements on the solids were conducted using a PTI QM-40, PLQY ultrasensitive fluorimeter system containing a 6-in. integrating sphere (K-Sphere B) redesigned for enhanced measurement of quantum yields of solids, films, and powders. The system includes dedicated quantum yield calculation functions. Wavelength selection is conducted by software controlled excitation and emission monochromators. The QY measurements were conducted on finely ground solids uniformly spread onto the sample holder and covered with a quartz disk.

RESULTS AND DISCUSSION

Structures of the One-Dimensional Polymers 1A, 1B, and 2. All three of these compounds are characterized by one-dimensional chain topologies formed from the bridging of Tb^{3+} cations by cis-bridging tetracyanoplatinate anions. Details of the structure types of **1A** and **1B** have been given elsewhere for the isostructural Eu[41] and Yb[46] compounds, respectively. Although **2** contains the 4′-chloro-2,2′:6′,2″-terpyridine ligand, it is interestingly isomorphous with **1B**.

Each of these structures consist of neutral, one-dimensional $^1_\infty\{Tb(C_{15}H_{10}XN_3)(H_2O)_2(NO_3)Pt(CN)_4\}$ (X = H, Cl) chains in addition to unbound solvate molecules. Depictions of the chain structures for all three compounds are shown in Figure 1 for comparison. The chains are formed by the linkage of the Tb^{3+} cations by cis-bridging tetracyanoplatinate (TCP) anions, and the Tb coordination is a 9-fold $[TbO_4N_5]$ distorted tricapped trigonal prism for all three compounds. One tridentate terpy (**1A** or **1B**) or terpy-Cl (**2**) ligand and two N-bound TCP anions account for the bound N atoms while the Tb^{3+} is additionally bound by one bidentate nitrate anion and two coordinated water molecules.

The packing diagram of **1A** along the crystallographic c axis (parallel to the one-dimensional chains) is shown in Figure 2 and can be contrasted with the chain arrangement of **1B** and **2**, shown in Figure 3. While the formulation for these chains looks quite similar, the structural topologies are markedly different in regards to chain orientation. The former compound contains an alternating arrangement of the terpy ligands as propagation along the chain proceeds, as observed in the isostructural compound containing the larger Eu^{3+} cation.[41] However, both of the latter compounds display a different type of chain structure, where the terpy or terpy-Cl molecules reside solely on one side of the chain. This type of chain structure is known

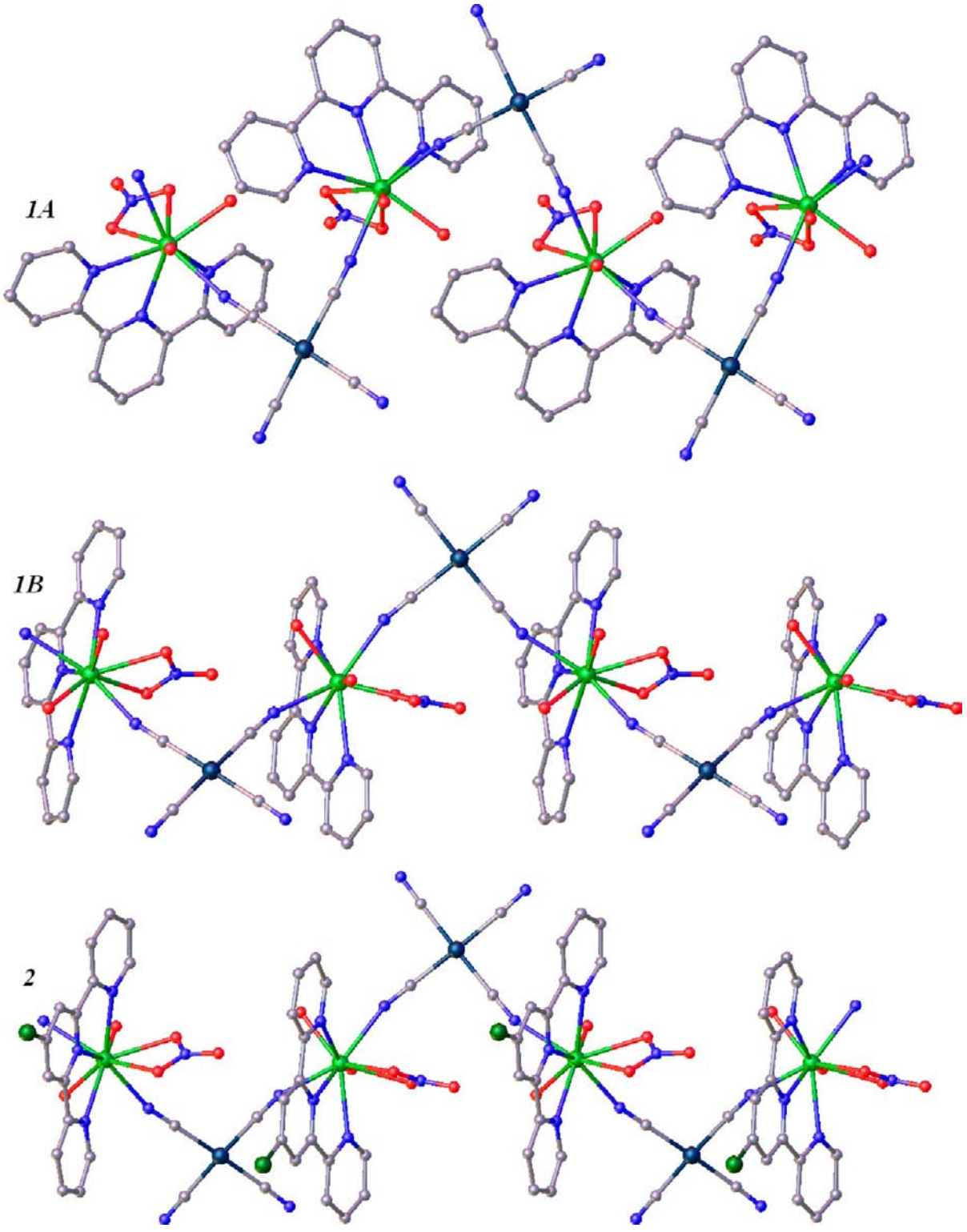

Figure 1. Representation of the one-dimensional chains in **1A**, **1B**, and **2**.

for compounds of smaller lanthanides, for example, Yb^{3+}.[46] Isolation of both chain types with Tb^{3+} likely results because of its intermediate size relative to Eu^{3+} and Yb^{3+}.[47]

A predominant interchain feature in each compound is the existence of platinophilic, Pt···Pt, interactions. As described earlier,[48] these interactions have strengths comparable to hydrogen bonds and often direct the structures of compounds that contain them. The interchain Pt···Pt interactions are weakest for **1A** and strongest for compound **2**, as illustrated by their bond distances given in Table 2. However, all of these platinophilic interactions are relatively weak with distances greater than 3.4 Å. Additionally, the observation of discrete Pt_2 dimers is a similarity for all of these polymeric structures. This is in contrast to what is normally observed in tetracyanoplatinate structural chemistry in which the structures are often characterized by simulated one-dimensional chains of planar

dx.doi.org/10.1021/ic3013975 | *Inorg. Chem.* 2012, 51, 12230−12241

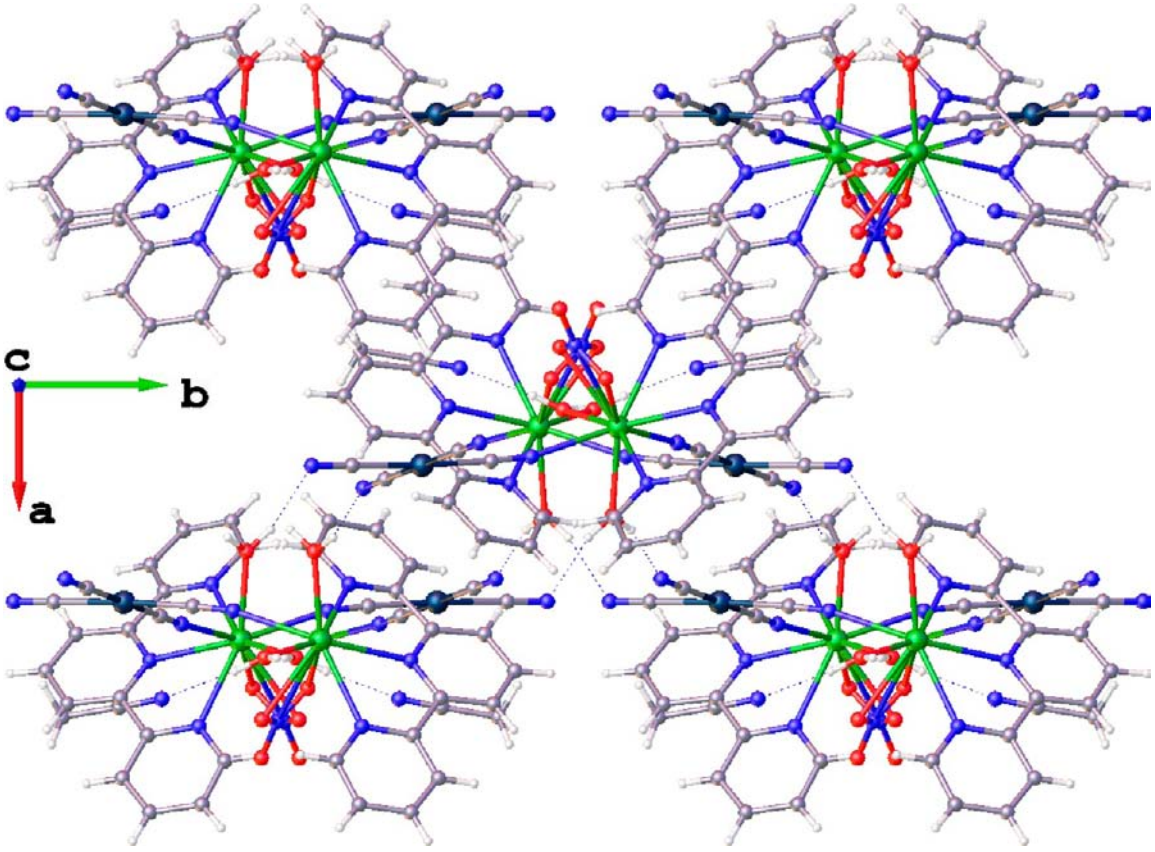

Figure 2. Packing diagram for **1A** viewed along the *c* axis, the direction parallel to the 1-D chains. H-bonding interactions are shown by the dashed lines. Tb atoms are shown in light green, Pt atoms in purple, Cl in dark green, C in gray, N in blue, and O in red.

TCP anions.[18−21,49,50] For example, $Er_2[Pt(CN)_4]_3\cdot 21H_2O$[49] contains TCP stacks with nonequidistant Pt···Pt separations of 3.1625(5) and 3.1891(3) Å, while $BaPt(CN)_4\cdot 4H_2O$[50] contains Pt···Pt distances of 3.321(3) Å in its stacks.

Strong interchain H-bonding is an additional noncovalent interaction found in all of these polymeric structure types. The water donors interact strongly, in particular, with the cyanide acceptors of adjacent chains. Additionally, compounds **1B** and **2** contain relatively strong π-stacking interactions as illustrated by Figure 4, a view normal to the interacting pyridine rings. While optimum ring overlap is not present in either structure, the centroid-plane distances for **1B** are ∼3.56 Å and therefore constitute consideration as an important interaction. Compound **2**, which is isomorphous to **1B**, contains the same type of π-stacking interactions with slightly reduced distances of ∼3.53 Å. In contrast, the 1-D chains in **1A** orient in such a fashion as to preclude the formation of any π-stacking interactions.

Several general conclusions are evident from the average atomic distances listed in Table 2. For the polymers **1A**, **1B**, and **2**, the two longest Tb−O bond distances are those to the nitrate anion while the Tb−O distances to the coordinated water molecules are considerably shorter. The Tb−O distances to the chelated acetate anions in **3** and **4** are shorter than the Tb−O(NO_3) bonds in the polymers. These distances are in line with literature values; for example, the Tb−O(NO_3) distances to bidentate nitrate anions average 2.483(3) Å in $[Tb(terpy)(acac)(NO_3)_2]$[51] and the Tb−O($CH_3COO$) bond distances between Tb^{3+} and the chelated acetate anions in $[Tb(bidc)(CH_3COO)\cdot H_2O]_n$ (H_2bidc = benzimidazole-5,6-dicarboxylic acid)[52] have an average value of 2.486(4) Å. A distinction in the distances for the Tb−N bonds to the cyano groups and the Tb−N bonds to the terpy or terpy-Cl moieties is also evident; the Tb−N bonds to the latter are longer by ∼0.06 Å, a trend also observed in the related Eu compounds.[41] Additional details of atomic distances can be found in Table 2 and the Supporting Information.

Structures of Complex Salts 3 and 4. In contrast to the polymeric features of **1A**, **1B**, and **2**, the structures of **3** and **4** can best be described as ionic salts formed from the crystallization of large, complex cations and $Pt(CN)_4^{2-}$ anions. The reduction in structural dimensionality can be ascribed to the multiple coordinated acetate anions in the cations, $[Tb(C_{15}H_{11}N_3)(H_2O)_2(CH_3COO)_2]^+$ in **3** or $[Tb_2(C_{15}H_{11}N_3)_2(H_2O)_2(CH_3COO)_5]^+$ in **4**. Two such cations crystallize with one uncoordinated TCP anion in each of these structures. Whereas only one nitrate anion binds each Tb^{3+} in the polymers, the more strongly coordinating acetate anions tie up four and five coordination sites in **3** and **4**, respectively, effectively excluding the bridging TCP anions from coordinating the terbium ions and thus rendering the compounds as zero-dimensional.

Figure 5 gives a ball and stick depiction of **4**, including one $[Tb_2(C_{15}H_{11}N_3)_2(H_2O)_2(CH_3COO)_5]^+$ cation and one TCP anion, only half of which is included in the asymmetric unit. Each Tb^{3+} site in the complex cation contains coordination by one terpy, two chelating acetate anions, and one water molecule. Additionally, one bridging acetate anion links the two Tb^{3+} positions together, along with added structural rigidity from several intracation H-bonds between the

dx.doi.org/10.1021/ic3013975 | *Inorg. Chem.* 2012, 51, 12230−12241

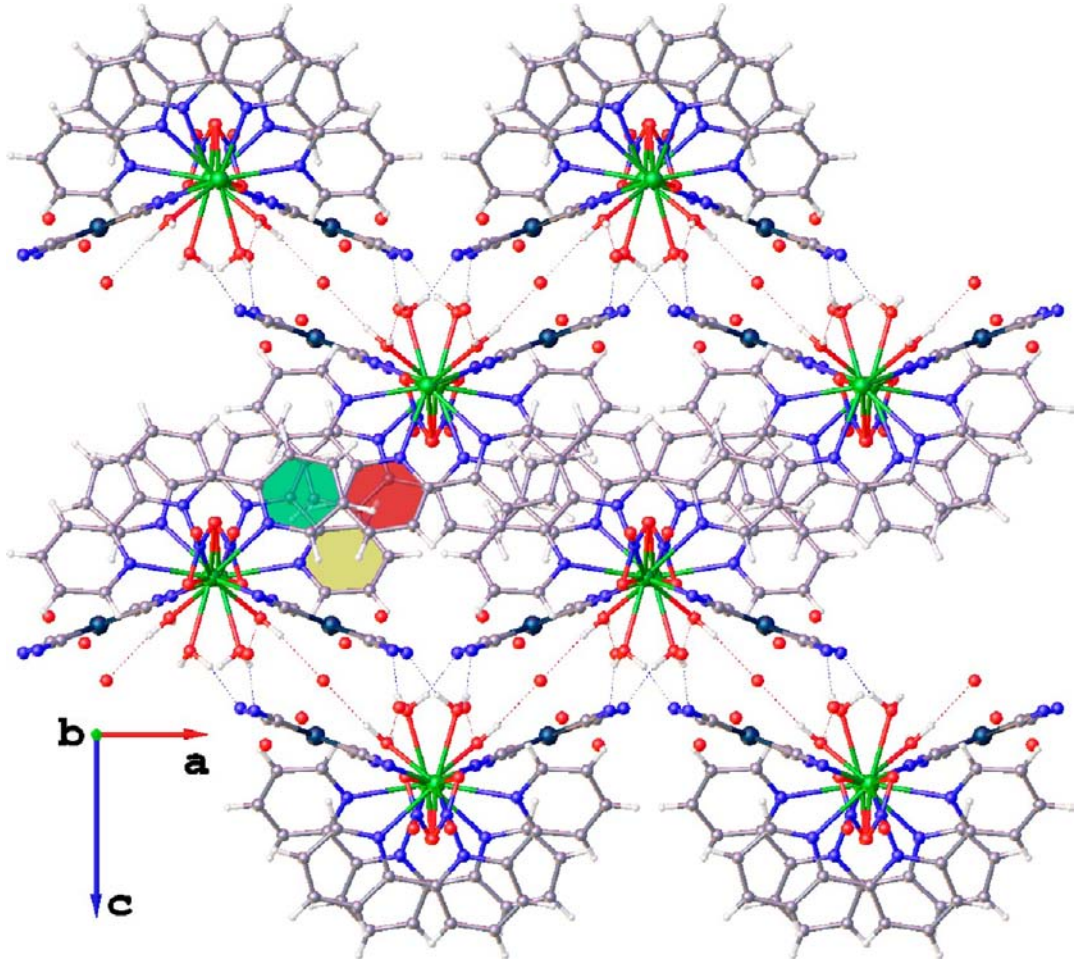

Figure 3. Packing diagram for **1B** viewed along the *b* axis, the direction parallel to the 1-D chains. H-bonding interactions are shown by the dashed lines, and the three pyridine rings are highlighted in different colors. Tb atoms are shown in green, Pt atoms in purple, C in gray, N in blue, and O in red.

Table 2. Average Atomic Distances (Å) for $Tb(C_{15}H_{11}N_3)(H_2O)_2(NO_3)Pt(CN)_4 \cdot CH_3CN$ (1A), $Tb(C_{15}H_{11}N_3)(H_2O)_2(NO_3)(Pt(CN)_4) \cdot 3.5H_2O$ (1B), $Tb(tpy\text{-}Cl)(H_2O)_2(NO_3)[Pt(CN)_4] \cdot 2.5H_2O$ (2), $[Tb(C_{15}H_{11}N_3)(H_2O)_2(CH_3COO)_2]_2Pt(CN)_4 \cdot 4H_2O$ (3), and $[Tb_2(C_{15}H_{11}N_3)_2(H_2O)_2(CH_3COO)_5]_2Pt(CN)_4 \cdot 7H_2O$ (4)

abbreviation	1	1B	2	3	4
Tb−N(tpy)	2.546	2.527	2.542	2.553	2.548
Tb−N(TCP)	2.478	2.476	2.482	N/A	N/A
Tb−O(H_2O)	2.376	2.386	2.372	2.394	2.374
Tb−O(NO_3)	2.512	2.502	2.506	N/A	N/A
Tb−O(bridging CH_3COO)	N/A	N/A	N/A	2.445	2.317
Tb−O(chelating CH_3COO)	N/A	N/A	N/A	N/A	2.465
Pt−C	1.992	1.987	1.987	1.987	1.981
C−N(terminal cyanide)	1.136	1.140	1.144	1.142	1.151
C−N(bridging cyanide)	1.142	1.146	1.144	N/A	N/A
C−Cl	N/A	N/A	1.728	N/A	N/A
Pt···Pt	3.562	3.431	3.402	9.054	11.477

coordinated water of a terbium cation to one of the coordinated acetates of the opposing terbium cation, as shown in Figure 5. The structure of **3** is related to that of **4**, as the coordination environments of the Tb^{3+} cations are very similar. Replacement of the bridging acetate in **4** with two terminal water molecules in **3** constitutes the major difference between the complex cations in these structures. Charge balancing by one TCP anion per two complex cations and addition of additional uncoordinated lattice waters completes the crystal structures for these compounds.

In terms of noncovalent interactions, **3** and **4** both contain H-bonding and π-stacking interactions. The latter interactions appear to be somewhat stronger relative to the polymers in terms of overall number of interactions, average ring overlap, and distance (from 3.3 to 3.6 Å). A significant difference in the structure of **3** and **4** relative to the polymers is the complete absence of any platinophilic interactions in both of the former.

dx.doi.org/10.1021/ic3013975 | *Inorg. Chem.* 2012, 51, 12230−12241

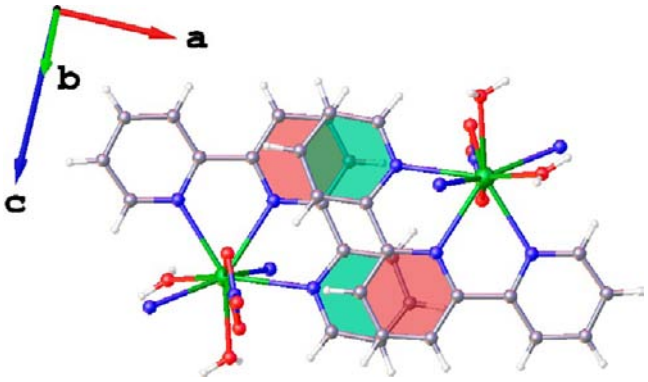

Figure 4. Ball and stick representation of the π-stacking interactions in **1B**. Since **2** is isomorphous with **1B**, it contains the same type of π-stacking interactions.

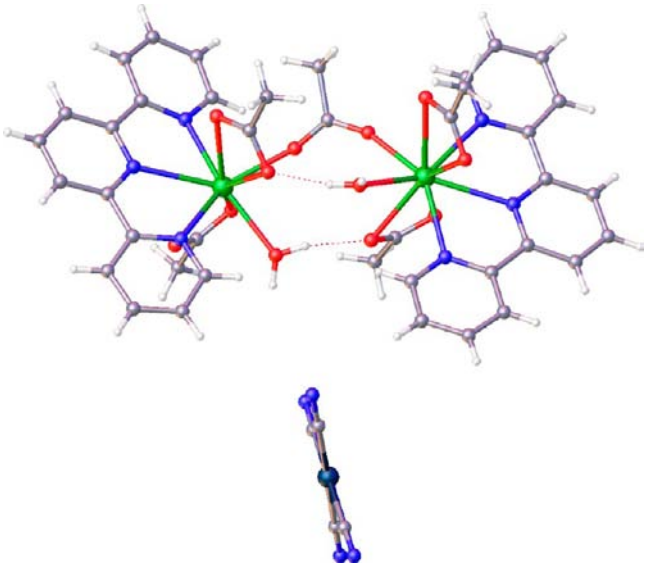

Figure 5. Ball and stick representation of the dimeric structure of the cation in **4**. Tb atoms are shown in green, Pt atoms in purple, C in gray, N in blue, and O in red.

As shown in Table 2, the shortest distance between any two Pt atoms in these salts is greater than 9 Å, much too long to be considered of any importance. The large separation between the Tb^{3+} and TCP moieties in **3** and **4** has implications on the observed luminescence properties as described in the spectroscopic discussion below.

Photoluminescence (PL) Studies. *PL Studies of 1A and 1B.* Figure 6 shows the emission and excitation spectra of **1A** collected at 77 K. When excited at 340 nm, a broad-band emission that maximizes at 455 nm is observed, and contains a shoulder at 412 nm. In addition, dominant and sharp bands characteristic of the Tb^{3+} ion f–f transitions are observed at 489, 541, 545, 582, 590, 621, and 647 nm. These bands are assignable to transitions originating from the $^5D_4$ to ^7F_J states. The most intense band in this group is observed at 541 nm, followed by the one at 489 nm. Overall the Tb^{3+} emission intensities are much stronger than the broad-band emission, which is assigned to the TCP unit. Changing the excitation wavelength to 370 nm significantly affects the overall emission profile. Although no major shift in band position is observed, the emission intensity of the TCP unit increases by more than 5-fold when compared with the 340 nm excitation, while the

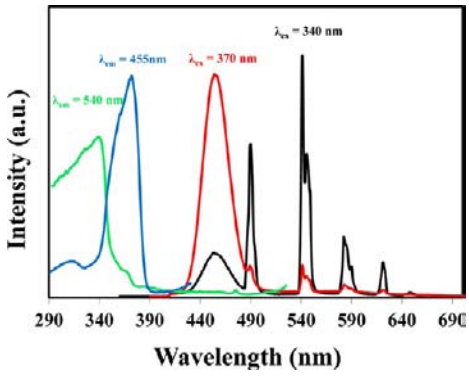

Figure 6. Wavelength dependent emission spectra of **1A** and excitation spectra of **1A** monotored at the Tb^{3+} (540 nm) and the TCP (455 nm) emission bands. All spectra were collected at 77 K.

Tb^{3+} emission decreases by more than 6-fold. Overall, the ratio of the TCP:Tb^{3+} emission intensities are 0.4:1, 10.5:1, and 22:1 for the 340, 360, and 370 nm excitations, respectively. Figure 6 also contains the excitation spectra of **1A** collected at room temperature. A comparison is shown for the excitation monitored at the Tb^{3+} (540 nm) and the TCP (455 nm) emission bands. The two emissions clearly display independent excitation profiles, suggesting a lack of communication between the excited states responsible for the emissions. When monitored at the Tb^{3+} line, the excitation spectrum is dominated by a broad band that maximizes at ~340 nm. The broadness of the band as well as previous reports on similar compounds suggest that the 340 nm broad band is likely associated with the terpy ligand.[41] In contrast the TCP emission shows an excitation profile with an intense broad band that maximizes at 371 nm and a very weak, broad band at ~310 nm. In addition, weak sharper bands assignable to Tb^{3+} f–f transitions are also evident at 381 and 475 nm.

The excitation and emission spectra for **1B** collected at 77 K are shown in Figure 7. The emission spectra were collected

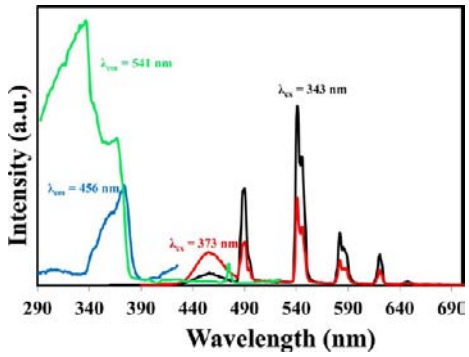

Figure 7. Excitation and emission spectra of **1B** at 77 K.

upon excitation at 343 and 373 nm. Similar to the profile described above for **1A**, two features dominate the spectra. A relatively weak and broad TCP band is observed at 456 nm and the Tb^{3+} f-f transitions are observed at their characteristic positions. For 343 nm excitation, the Tb^{3+} emissions are dominant by at least 10-fold when compared with the TCP emission. Like the situation observed in **1A**, the observation of strong Tb^{3+} based emissions upon ~343 nm excitation demonstrates that the sensitized emission is achieved through the terpy antenna states. Excitation at lower energy provides a

dx.doi.org/10.1021/ic3013975 | *Inorg. Chem.* 2012, 51, 12230–12241

spectral profile similar to that exhibited in **1A**, where TCP emission dominates with a concomitant decrease of the Tb^{3+} emission. Moreover, temperature dependent behavior is observed in the TCP band in **1B**, where at room temperature the band blue shifts by ~1000 cm^{-1} and is observed at 436 nm. The temperature dependent shift in the emission profile is a known phenomenon in platinum and gold complexes that display expansion in M−M distances with a temperature increase.[53] Hence, the phenomenon is suggestive of M−M character in the electronic transition as is discussed in a later section.

The excitation spectra of **1B** collected at 77 K are also shown in Figure 7. These spectra exhibit a very similar profile to those of **1A**, where monitoring the excitation at the TCP (456 nm) and Tb^{3+} (541 nm) emission bands provide drastically different profiles. A longer wavelength band is dominant for the former, while the most intense excitation band upon monitoring the Tb^{3+} line is observed at ~335 nm, a band totally absent in the TCP spectrum. The excitation spectra of **1B** at room temperature also show similar behavior to that seen in the liquid N_2 spectra where the Tb^{3+} and the TCP emissions display their own characteristic features. In fact, in the wavelength region where the Tb^{3+} excitation maximizes, the TCP profile shows a minimum, indicating a lack of communication between the two excited states.

PL Studies of 2. The excitation-dependent emission spectra of **2** recorded at 77 K and room temperature are shown in Figure 8. When compared to the spectra of **1A** and **1B**, a major

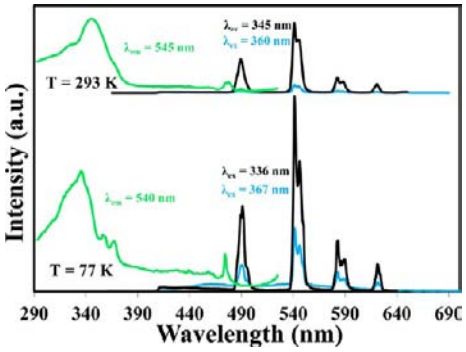

Figure 8. Emission spectra of **2** at room temperature and 77 K.

difference is that at room temperature the broad band TCP emission is quenched and the Tb^{3+} f-f transitions are dominant. At 77 K, weak and broad profiles are observed at ~460 and ~540 nm when **2** is excited at 367 nm. The broad bands overlay with the Tb^{3+} lines and as a result the peak maxima are not clearly defined. When the excitation wavelength is changed to 336 nm, the intensity of the broad band emission is negligible, while the Tb^{3+} emission is enhanced by nearly 3-fold. In contrast the room temperature data lacks the broad TCP emission at all excitation wavelengths used.

PL Studies of 3 and 4. The major structural consequences of the incorporation of the acetate ion in **3** and **4** are (1) the removal of direct bonding between the cyanide groups of the tetracyanoplatinate anion and the Tb^{3+} ion, and (2) the lack of platinophilic interactions. Both of these contrast the structural features present in **1A**, **1B**, and **2**. Additionally, both **3** and **4** are not polymeric, but rather ionic in nature. These structural differences affect the overall emission profiles in terms of band position, relative intensity, and temperature dependency as compared with the polymeric compounds.

The room temperature spectra of **3** in Figure 9 show the excitation-dependency of the emission profile. Excitation at 340

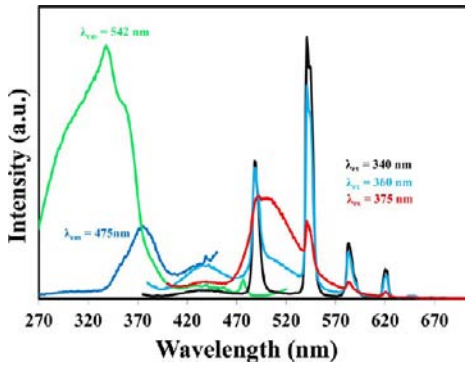

Figure 9. Room temperature excitation and emission spectra of **3**.

nm provides a weak broad emission at ~440 nm and strong characteristic Tb^{3+} emissions. The intensity of the broad band increases along with a profile change as the excitation wavelength moves to longer wavelengths. At 360 nm excitation another broad band emerges in the 500 nm region overlaying with the Tb^{3+} band at 488 nm. The 440 nm broad band is also well-defined at this excitation wavelength. Shifting the exciting wavelength to 370 nm reduces the Tb^{3+} emission intensity significantly and the broad band at ~500 nm becomes dominant. At 77 K however, the profile at 500 nm is weak and only the 450 nm band remains strong within the 336 to 370 nm excitation range.

Figure 9 also contains the excitation spectra of **3** collected at RT. When monitored at the Tb^{3+} emission (542 nm), the excitation spectrum exhibits a very broad feature covering the 260−400 nm region with sharp overlay at 340 nm and broader shoulders at ~300 and 355 nm. On the other hand, when the excitation is monitored at 475 nm the broad profile changes drastically and a less intense band is observed at a red-shifted position of ~370 nm. The overall profile clearly indicates that the two emitting states have little communication between them. The broad band covering the 280−400 nm region is assignable to the coordinated ligands where a combination of terpy and the acetate groups are involved in the sensitization processes. In contrast, the TCP group has its own distinct feature at ~370 nm, which is not coupled with the Tb^{3+} emitting levels.

Similarly, the emission profile of **4** shown in Figure 10 is quite similar to that observed for **3**, where excitation at 343 nm provides the very intense Tb^{3+} emission with a weak band appearing at ~450 nm. The intensity of this band increases when the excitation wavelength shifts to 360 nm and another broad band appears at ~500 nm overlaying with the Tb^{3+} emission. This broad band is clearly defined and, with a concomitant reduction of the Tb^{3+} emission, becomes the most dominant at 380 nm excitation. A similar profile is repeated at 77 K as shown in the bottom spectra of Figure 10.

Comparison with the Eu-Terpy-TCP Systems. The terbium compounds reported here have similar structural features with those reported for several related europium systems.[41] However, the PL properties of these two classes of compounds are quite different indicating the complexity of the spectral profiles and the energy transfer modes in the systems.

dx.doi.org/10.1021/ic3013975 | *Inorg. Chem.* 2012, 51, 12230−12241

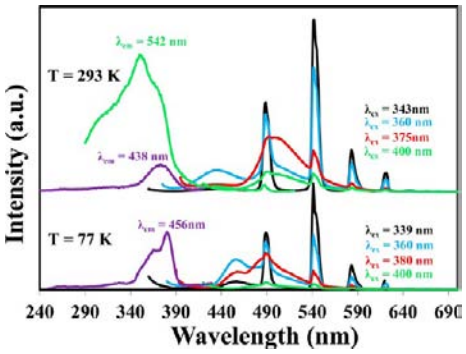

Figure 10. Emission spectra of **4** at room temperature and 77 K.

Although the Eu^{3+} analogue of **1A**, $\{Eu(C_{15}H_{11}N_3)(H_2O)_2(NO_3)Pt(CN)_4\}\cdot CH_3CN$, **Eu1**,[41] is characterized by a lack of emission assignable to TCP, a broad band indicative of TCP is prevalent in most of the Tb^{3+} compounds reported herein. These findings suggest contrasting ET modes between the two systems, where efficient energy transfer is inferred in the former and lack of energy transfer in the latter. It is found that the dominance of the TCP based bands vary among the Tb^{3+} compounds studied in this work. For example, in **1A** two distinct excitation maxima provide dominant TCP emissions when excited at 380 nm, and the Tb^{3+} emission maximizes upon excitation at 340 nm. This trend is evident in **1B** where the TCP band at 430 nm is not as dominant as the profile observed in **1A**.

Compound **2** which contains the Cl-substituted terpy ligand (terpy-Cl), is characterized by a lack of TCP features in its room temperature emission profile, while displaying two weak and broad bands at 430 and 540 nm in the 77 K spectrum. The three compounds (**1A**, **1B**, and **2**) are structurally similar in that they all display a dimeric Pt···Pt interaction of varying degree, with the longest interaction present in **1A**. As shown in Table 2, the Pt···Pt distances are 3.562, 3.431, and 3.402 Å in **1A**, **1B**, and **2**, respectively. In addition, compounds **1B** and **2** also display additional extended π-stacking of the terpy units, while **1A** lacks such interactions.

The influence of these minor structural differences on the overall emission behavior has been analyzed to understand the ET mechanism involved in these systems. A common feature evident in all of these compounds is the observation of a broad excitation band in the 320−370 nm region when monitored at the Tb^{3+} emission lines. Observation of this broad band upon monitoring the Tb^{3+} emission is indicative of ET from a terpy-based donor to the Tb^{3+} acceptor species and that the sensitization is relatively efficient within this series of compounds.

As discussed above, lack of TCP involvement in the ET process is clearly evident when the excitation profile obtained by monitoring the TCP band (at 450 nm) is compared with that of the Tb^{3+} band. The two profiles are entirely different and it can be concluded that the ET process from the TCP donor to the Tb^{3+} acceptor state is inefficient. On the other hand, the spectral profiles of **1A** and **1B** indicate that energy transfer from the terpy ligand to the Tb^{3+} takes place efficiently, as is the case with the Eu^{3+} compound isostructural with **1A**, $\{Eu(terpy)(H_2O)_2(NO_3)Pt(CN)_4\}\cdot CH_3CN$, (**Eu1**).[41]

While compounds **1A** and **1B** display TCP emission at ~440 nm, **2** lacks this emission at room temperature but emits weakly at 77 K. Similarly, compounds **3** and **4** display a broad band at 440 nm, in addition to a more intense broad band at ~500 nm. The band at ~440 nm is assignable to a MLCT transition within the $Pt(CN)_4^{2-}$ unit. In support of this assignment, the Eu^{3+} analogue of **3**, $[Eu(terpy)(H_2O)_2(CH_3COO)_2]_2Pt(CN)_4\cdot 4H_2O$, **Eu3**, shows[41a] TCP emission at exactly the same position.

A characteristic feature of these transitions is that the emission increases in intensity as the excitation wavelength approaches a maximum value of 380 nm. The absence of platinophilic interactions in **3** and **4** clearly infers minimal influence of a metal-metal-to-ligand charge-transfer (MMLCT) transition that arises when relatively short Pt···Pt interactions (~3−3.5 Å) exist. In fact, even in **1A** the dimeric Pt···Pt contact is outside of this margin. In contrast, the metal-to-ligand charge-transfer (MLCT) transition of $[Pt(CN)_4]^{2-}$ consists of higher energy absorption and emission[21] when compared with the MMLCT. Hence the compounds with isolated $[Pt(CN)_4]^{2-}$ such as in **3** and **4** are expected to have transitions assignable to MLCT bands. It is thus reasonable to assign the band at ~440 nm to the ^{1}MLCT while the longer wavelength band exhibited in both **3** and **4** at ~500 nm can be assigned to a ^{3}MLCT transition within the TCP unit. Although the absence of strong *extended* Pt···Pt interactions in all of the compounds studied herein precludes the prevalence of MMLCT transitions, which would have been expected at longer wavelengths, compounds **1B** and **2** in particular have relatively short dimeric Pt···Pt interactions that may play a role in influencing their overall spectroscopic profiles. This topic is discussed further in the following section.

Photophysical Analysis and Energy Transfer Kinetics for the Eu^{3+} Systems. Insight into the relevant radiative and nonradiative parameters were deduced from the luminescence spectra of the compounds, quantum yield, and lifetime data. Standard interpretation was followed by adapting the works of Werts et al.[54] and Beeby et al.[55,56] The overall quantum yield, φ_{lum}, as given in eq 1 depends on the triplet yield of the chromophore (ϕ_T), the energy transfer efficiency (η_{ET}), and the efficiency of the intrinsic metal centered luminescence (η_{Ln}).

$$\varphi_{lum} = \phi_T \cdot \eta_{ET} \cdot \eta_{Ln} \quad (1)$$

The presence of a purely magnetic dipole allowed $^5D_0 \rightarrow {}^7F_1$ transition in Eu^{3+} systems is known to simplify the estimation of the τ_{rad} value in its complexes since the oscillatory strength of the transition is virtually independent of the ligand field and complex symmetry. Hence, we have presented the photophysical data analysis of the Eu^{3+} systems.

The efficiency of the metal centered emission η_{Ln} (eq 2) can be calculated from the ratio of the observed emission and radiative lifetimes, which in turn is easily calculated for the

$$\eta_{Ln} = \tau_{obs}/\tau_{rad} \quad (2)$$

Eu^{3+} system using eq 3. Knowledge of the spontaneous emission probability of the $^5D_0 \rightarrow {}^7F_1$ transition ($A_{(0,1)}$) is the only factor needed to use the experimental emission intensities in the calculation of the overall radiative quantity $A_{(0,J)}$ in eq 3.

$$A_{(0,J)} = A_{(0,1)} \sum_J \frac{I_{0,J}}{I_{0,1}} \frac{\upsilon_{0,1}}{\upsilon_{0,J}} \quad (3)$$

Where $A_{(0,J)}$ is the radiative transition rate and $A_{(0,1)}$ is the magnetic dipole transition rate which is estimated to be 50 s^{-1} for solids.[57] The value $I_{0,J}/I_{0,1}$ corresponds to the ratio of the integrated emission intensity obtained from the corrected

dx.doi.org/10.1021/ic3013975 | Inorg. Chem. 2012, 51, 12230−12241

emission profile, and υ corresponds to the frequency of the corresponding $^5D_0 \rightarrow {}^7F_J$ transition energies. A_{rad} is then obtained after summing over the radiative rates for each of the $^5D_0 \rightarrow {}^7F_J$ transitions. Finally the efficiency of sensitization upon donor excitation is calculated by using eq 4.

$$\eta_{ET}{}^{L} = \varphi_{lum}/\eta_{Ln} \quad (4)$$

The photophysical values calculated based on the above approach for $\{Eu(C_{15}H_{11}N_3)(H_2O)_2(NO_3)Pt(CN)_4\}\cdot CH_3CN$ (**Eu1**), $\{Eu(C_{15}H_{11}N_3)(H_2O)_3\}_2(Pt(CN)_4)_3\cdot 2H_2O$ (**Eu2**), and $[Eu(terpy)(H_2O)_2(CH_3COO)_2]_2Pt(CN)_4\cdot 4H_2O$ (**Eu3**)[41] are listed in Table 3. Although there is a significant overlap between the absorption profiles of the two donors, terpy and TCP, the longer wavelength side mostly consists of contribution from the latter and the shorter wavelength side from the former. Hence, dependence of the QY data on the excitation wavelength was evident. With the 370 nm excitation (mostly the TCP unit), the quantum yield values for compounds **Eu1** and **Eu2** are almost identical (4.1 and 4.2%, respectively), while a reduction by ∼40% is observed for **Eu3** (2.6%), indicating the diminished contribution from the TCP unit in the ET process. The overall nonradiative rate, k_{nr}, increased by ∼30% on going from **Eu1** to **Eu2**, presumably because of the additional H_2O coordinated in **Eu2**.

Table 3. Photophysical Data of the Eu^{3+} Compounds

comp.	$^a\phi_{lum}$ (%)	τ_{obs} (ms)	τ_r (ms)	k_r (10^2 s^{-1})	k_{nr} (10^3 s^{-1})	$\eta_{Eu}{}^{M}$	$\eta_{Eu}{}^{L}$
Eu1	4.1	0.42	3.73	2.68	2.11	0.11	0.37
Eu2	4.2	0.36	3.3	3.0	2.74	0.11	0.38
Eu3	2.6	0.46	3.18	3.14	1.86	0.14	0.19

[a]Quantum yield data for λ_{ex} = 370 nm which provides more contribution from the TCP donor excitation.

In **Eu3**, the non radiative rate (1.86×10^3 s^{-1}) is significantly reduced by 30% when compared with that of **Eu2**, and the intrinsic emission efficiency has increased to 14%. However, the diminished contribution of the TCP unit in the overall sensitization in **Eu3** is apparent from analysis of the energy transfer data. As shown in Table 3, the $\eta_{ET}{}^{L}$ value is only 19% for **Eu3** compared to 37 and 38% for **Eu1** and **Eu2**, respectively.

In contrast, similar analysis for the 340 nm wavelength excitation, which is largely terpy based, is different in that the energy transfer efficiency, η_{ET}, in **Eu3** is 76% compared to 54 and 48% for **Eu1**, and **Eu2**, respectively. The larger overall efficiency of the energy transfer process in **Eu3** upon terpy excitation is attributable partly to the increased efficiency of the intrinsic metal based emission and the reduced nonradiative process when compared to **Eu1** and **Eu2**.

Hence, the situation requires careful monitoring of the balance in counterion choice, removal of ν_{OH} high vibrational manifolds, the type of auxiliary ligand used for complex stability, and the extent of overlap of the dual donor absorptions as well as matching of photophysical properties in terms of donor−acceptor excited energy levels and lifetime values.

Quantum Yield (QY) of the Tb Complexes. Analysis of the photophysical data of the Tb^{3+} complexes has not been as straightforward as that of the Eu^{3+} system because of the absence of an intense purely magnetic dipole transition that can be considered as purely radiative. As a result, the analysis of the existing data could not establish the transition probabilities and efficiencies of the sensitization process in these systems. Nevertheless, the excitation-dependent QY data for compounds **1A**, **1B**, **2**, and **3** are given in Table 4. The general trend as shown for **1A** is that as the excitation wavelength increases (between 330−380 nm) the QY of the Tb^{3+} emission decreases, while that of the TCP emission increases. As shown in Table 4, the 340 nm excitation has QY values of 7.6 and 1.9% for the Tb^{3+} and TCP emissions, respectively. Similarly, the QY of the Tb^{3+} emission decreases to 2.7 and 0.8% when excited at 370 and 380 nm, respectively. In contrast, the corresponding values for the TCP emissions are 8.8 and 17.5% indicating the dominance of TCP emission upon longer wavelength excitation. Compared to **1A**, the QY of the Tb^{3+} emission in **1B** increases by nearly 3-fold. This observation requires explanation since the coordination mode around the Tb^{3+} in the two compounds is similar in terms of ligand type and coordination number; thus, similar quantum yield values would have been expected.

Comparison of the TCP excitation profiles for the two compounds indicates that spectral overlap in **1B** is stronger than in **1A**. In addition, **1B** displays a shorter Pt···Pt interaction than **1A** and as a result may induce a better energy match up with the Tb^{3+} acceptor state. The TCP emission is also highly quenched as can be implied from the QY value of 1.4% for **1B** versus 17.5% for **1A.** In addition, the TCP emission band shows a red shift at 77 K (456 nm) relative to room temperature (437 nm). Hence it is possible that a MMLCT transition originating from the shorter dimeric Pt···Pt interaction could be a factor in the energy transfer process of **1B**, although such a prospect is completely absent in **1A**.

Fine tuning of the ET process was achieved by using a chloro substituted terpy ligand in **2** that maximizes the QY of the acceptor emission to 24.5%. As can be noted from Table 3, the largest QY value for **2** is obtained at 360 nm, slightly red-shifted when compared with that of **1A** and **1B**. The structural profile of the system is also suggestive of a more complex feature in the ET mechanism. The presence of an electron withdrawing substituent in the central pyridine ring is expected to increase the energy position of the donor $^3\pi^*$ state and its overlap with the Tb^{3+} acceptor $^5G_6$ state. As a result, the overall QY significantly increases.

Table 4. Quantum Yield Data for the Tb^{3+} Compounds[a]

comp.	emitter	Φ (330 nm)	Φ (340 nm)	Φ (350 nm)	Φ (360 nm)	Φ (370 nm)	Φ (380 nm)
1A	Tb^{3+}/TCP	7.9/1.2	7.6/1.9	7.6/2.3	6.6/4.1	2.7/8.8	0.8/17.5
1B	Tb^{3+}/TCP	19.0/na	24.3/na	12.0/na	16.4/na	10.5/1.5	
2	Tb^{3+}	18.5	21.1	22.1	24.5	15	8.2
3	Tb^{3+}	14.0	13.3	14.5	11.7	10.4	5.8

[a]The excitation wavelength for the quantum yield data are given in parentheses.

dx.doi.org/10.1021/ic3013975 | Inorg. Chem. 2012, 51, 12230−12241

The QY value of **3** can also be used to glean the overall ET mechanism in this system. Considering the value found in **1A** as a reference point for the terpy contribution in the sensitization process, the 14.5% value obtained for **3** is suggestive of the presence of other factors that increase the overall quantum yield in the system. Since the isolated TCP unit has its own strong emission with a QY of 17.5%, it bears negligible contribution as a sensitizer of the Tb^{3+} unit. The increase observed in the QY of the Tb^{3+} ion in **3** most likely originates from the contribution of the acetate groups coordinated directly to the metal center. Support to this conclusion comes from the similar enhancement observed in the QY value of the Eu^{3+} analogue of **3**.[41]

The lifetime values for the Tb^{3+} complexes are shown in Table 5 for **1A**, **1B**, **2**, and **3**. The comparison indicates that compound **1B** has the shortest lifetime for the Tb^{3+} emission (330 μs) while **3** displays the longest lifetime (760 μs). In contrast the TCP emission has a much shorter lifetime of ~1 usec.

Table 5. Luminescence Lifetime and Photophysical Data for the Tb^{3+} Compounds

compound	emitter	λ (nm)	τ, μs
1A	Tb^{3+}	541	440
1A	TCP	435	1.0
1B	Tb^{3+}	541	330
2	Tb^{3+}	541	480
3	Tb^{3+}	541	760
3	TCP	435	0.85

SUMMARY AND CONCLUSIONS

Five novel terbium tetracyanoplatinates, each containing additional multidentate ligands on Tb^{3+}, have been synthesized and structurally characterized. Variation of the coordinating ability of the counteranions in the Tb^{3+} starting materials provides isolation of two drastic classes of structures. One-dimensional polymeric structure types are exhibited by **1A**, **1B**, and **2** which are prepared in reactions utilizing terbium nitrate as reactant. All three of these structures contain bridging of Tb^{3+} in a cis fashion by tetracyanoplatinate anions and interchain, dimeric platinophilic interactions. The structure analyses of **3** and **4**, prepared utilizing terbium acetate as reactant, reveal zero-dimensional ionic compounds containing no direct linkage between Tb^{3+} and tetracyanoplatinate and also no platinophilic interactions. The structural differences and concomitant changes in PL properties provide the opportunity to discern the ET mechanisms in these related systems. It is revealed that the sensitization phenomena vary drastically because of the structural differences. All of the compounds studied display efficient sensitization from the tridentate terpy ligand. Because of an energy mis-match, the TCP unit contribution in the energy transfer process is minimal in **1A**. In **1B** and **2** however, observance of stronger Pt···Pt interactions indicates weak involvement of a MMLCT transition in the energy transfer processes resulting in a dual-donor sensitization and a 3-fold increase of the QY for **1B** over **1A**. In **3** and **4**, which contain only uncoordinated TCP units, strong emission from TCP is present indicating a lack of energy transfer to Tb^{3+}. However, the quantum yield of Tb^{3+} is relatively high suggesting the existence of another dual donor system that contributes in the enhancement of the acceptor Tb^{3+} emission. It is indicative that the acetate ion is the likely sensitizer in addition to terpy.

ASSOCIATED CONTENT

Supporting Information

X-ray crystallographic data in CIF format. This material is available free of charge via the Internet at http://pubs.acs.org.

AUTHOR INFORMATION

Corresponding Author

*E-mail: zassefa@ncat.edu (Z.A.), rsykora@southalabama.edu (R.E.S.). Phone: (336) 285-2255 (Z.A.), (251) 460-7422 (R.E.S.).

Notes

The authors declare no competing financial interest.

ACKNOWLEDGMENTS

The authors gratefully acknowledge the National Science Foundation for their generous support (NSF-CAREER, CHE-0846680). Z.A. acknowledges support from the NOAA Educational Partnership Program award number NA06OAR4810187 to NCAT State University and support from the donors of the Petroleum Research Fund (ACS-PRF).

REFERENCES

(1) Bunzli, J.-C. G.; Piguet, C. *Chem. Soc. Rev.* **2005**, *34*, 1048−1077.
(2) Yam, V. W. W.; Lo, K. K. W. *Coord. Chem. Rev.* **1999**, *184*, 157−240.
(3) Aime, S.; Crich, S. G.; Gianolio, E.; Giovenzana, G. B.; Tei, L.; Terreno, E. *Coord. Chem. Rev.* **2006**, *250*, 1562−1579.
(4) Benelli, C.; Gatteschi, D. *Chem. Rev.* **2002**, *102*, 2369−2387.
(5) Crich, S. G.; Biancone, L.; Cantaluppi, V.; Duo, D.; Esposito, G.; Russo, S.; Camussi, G.; Aime, S. *Magn. Reson. Med.* **2004**, *51*, 938−944.
(6) Davies, G. M.; Pope, S. J. A.; Adams, H.; Faulkner, S.; Ward, M. D. *Inorg. Chem.* **2005**, *44*, 4656−4665.
(7) Aime, S.; Botta, M.; Parker, D.; Williams, J. A. G. *J. Chem. Soc., Dalton Trans.* **1996**, 17−23.
(8) Bunzli, J.-C. G. *Acc. Chem. Res.* **2006**, *39*, 53−61.
(9) dos Santos, C. M. G.; Fernandez, P. B.; Plush, S. E.; Leonard, J. P.; Gunnlaugsson, T. *Chem. Commun.* **2007**, 3389−3391.
(10) Castelli, D. D.; Gianolio, E.; Crich, S. G.; Terreno, E.; Aime, S. *Coord. Chem. Rev.* **2008**, *252*, 2424−2443.
(11) Faulkner, S.; Pope, S. J. A.; Burton-Pye, B. P. *Appl. Spectros. Rev.* **2005**, *40*, 1−31.
(12) Gunnlaugsson, T.; Stomeo, F. *Org. Biomol. Chem.* **2007**, *5*, 1999−2009 , and references therein.
(13) (a) Xu, H.-B.; Shi, L.-X.; Ma, E.; Zhang, L.-Y.; Wei, Q.-H.; Chen, Z.-N. *Chem. Commun.* **2006**, 1601−1603. (b) Chen, K.-J.; Xu, H.-B.; Zhang, L.-Y.; Chen, Z.-N. *Inorg. Chem. Commun.* **2009**, *12*, 744−746. (c) Ni, J.; Zhang, L.-Y.; Chen, Z.-N. *J. Organomet. Chem.* **2009**, *694*, 339−345.
(14) Coppo, P.; Duati, M.; Kozhevnikov, V. N.; Hofstraat, J. W.; DeCola, L. *Angew. Chem., Int. Ed.* **2005**, *44*, 1806−1810.
(15) (a) Figuerola, A.; Diaz, C.; El Fallah, M. S.; Ribas, J.; Maestro, M.; Mahia, J. *Chem. Commun.* **2001**, 1204−1205. (b) Figuerola, A.; Ribas, J.; Llunell, M.; Casanova, D.; Maestro, M.; Alvarez, S.; Diaz, C. *Inorg. Chem.* **2005**, *44*, 6939−6948.
(16) (a) Koner, R.; Drew, M. G. B.; Figuerola, A.; Diaz, C.; Mohanta, S. *Inorg. Chim. Acta* **2005**, *358*, 3041−3047. (b) Figuerola, A.; Ribas, J.; Solans, X.; Font-Bardia, M.; Maestro, M.; Diaz, C. *Eur. J. Inorg. Chem.* **2006**, 1846−1852.
(17) (a) Montalti, M.; Credi, A.; Prodi, L.; Gandolfi, M. T. *Handbook of Photochemistry*, 3rd ed., CRC Press, Taylor & Francis: Boca Raton, FL, 2006. (b) Juris, A.; Balzani, V.; Barigelletti, F.; Campagna, S.; Belser, P.; Von Zelewsky, A. *Coord. Chem. Rev.* **1988**, *84*, 85−277.

(c) Sauvage, J. P.; Collin, J. P.; Chambron, J. C.; Guillerez, S.; Coudret, C.; Balzani, V.; Barigelletti, F.; De Cola, L.; Flamigni, L. *Chem. Rev.* **1994**, *94*, 993−1019. (d) Bardez, E.; Devol, I.; Larry, B.; Valeur, B. *J. Phys. Chem. B* **1997**, *101*, 7786−7793. (e) Samuel, A. P. S.; Moore, E. G.; Melchior, M.; Xu, J.; Raymond, K. N. *Inorg. Chem.* **2008**, *47*, 7535−7544. (f) Moore, E. G.; Xu, J.; Jocher, C. J.; Castro-Rodriguez, I.; Raymond, K. N. *Inorg. Chem.* **2008**, *47*, 3105−3118.
(18) Yersin, H.; Stock, M. *J. Chem. Phys.* **1982**, *76*, 2136−2138.
(19) Yersin, H. *J. Chem. Phys.* **1978**, *68*, 4707−4713.
(20) Yersin, H.; von Ammon, W.; Stock, M.; Gliemann, G. *J. Lumin.* **1979**, *18*−*19*, 774−778.
(21) Gliemann, G.; Yersin, H. *Struct. Bonding (Berlin)* **1985**, *62*, 87−153 , and references therein.
(22) Daniels, W.; Yersin, H.; Philipsborn, H. V.; Gliemann, G. *Solid State Commun.* **1979**, *30*, 353−355.
(23) (a) Ammon, W.; von; Hidvegi, I.; Gliemann, G. *J. Chem. Phys.* **1984**, *80*, 2837−2844. (b) Ammon, W.; von; Gliemann, G. *J. Chem. Phys.* **1982**, *77*, 2266−2272.
(24) Hidvegi, I.; von Ammon, W.; Gliemann, G. *J. Chem. Phys.* **1982**, *76*, 4361−4369.
(25) Barnard, G. *Immunodiagnostics* **1999**, 137−158.
(26) Nanda, S.; Guardigli, M.; Manet, I.; Ziessel, R.; Lehn, J.-M. *Med., Biol., Environ.* **1995**, *23* (1), 101−107.
(27) Poole, R. A.; Montgomery, C. P.; New, E. J.; Congreve, A.; Parker, D.; Botta, M. *Org. Biomol. Chem.* **2007**, *5* (13), 2055−2062.
(28) Brunet, E.; Juanes, O.; Rodriguez-Ubis, J. C. *Curr. Chem. Biol.* **2007**, *1* (1), 11−39.
(29) Zang, F. X.; Li, W. L.; Hong, Z. R.; Wei, H. Z.; Li, M. T.; Sun, X. Y.; Lee, C. S. *Appl. Phys. Lett.* **2004**, *84* (25), 5115−5117.
(30) Zang, F. X.; Hong, Z. R.; Li, W. L.; Li, M. T.; Sun, X. Y. *Appl. Phys. Lett.* **2004**, *84* (14), 2679−2681.
(31) Okada, K.; Wang, Y.-F.; Chen, T.-M.; Kitamura, M.; Nakaya, T. *J. Mater. Chem.* **1999**, *9* (12), 3023−3026.
(32) Anderson, B. M.; Hurst, S. K. *Eur. J. Inorg. Chem.* **2009**, 3041−3054.
(33) Bozorth, R. M.; Pauling, L. *Phys. Rev.* **1932**, *39*, 537−538.
(34) Miller, J. S. *Extended linear chain compounds*; Plenum Press: New York, 1982; Vols. *1*−*3*.
(35) Rundle, R. E. *J. Phys. Chem.* **1957**, *61*, 45−50.
(36) Michalet, X.; Pinaud, F. F.; Bentolila, L. A.; Tsay, J. M.; Doose, S.; Li, J. J.; Sundaresan, G.; Wu, A. M.; Gambhir, S. S.; Weiss, S. *Science* **2005**, *307*, 538−544.
(37) Bukowski, T. J.; Simmons, J. H. *Crit. Rev. Solid State Mater. Sci.* **2002**, *27*, 119−142.
(38) Kolmakov, A.; Moskovits, M. *Annu. Rev. Mater. Res.* **2004**, *34*, 151−180.
(39) Comini, E.; Baratto, C.; Faglia, G.; Ferroni, M.; Vomiero, A.; Sberveglieri, G. *Prog. Mater. Sci.* **2009**, *54*, 1−67.
(40) Ladner, L.; Ngo, T.; Crawford, C.; Assefa, Z.; Sykora, R. E. *Inorg. Chem.* **2011**, *50*, 2199−2206.
(41) (a) Maynard, B. A.; Smith, P. A.; Ladner, L.; Jaleel, A.; Beedoe, N.; Crawford, C.; Assefa, Z.; Sykora, R. E. *Inorg. Chem.* **2009**, *48*, 6425−6435. (b) Maynard, B.; Kalachnikova, K.; Sykora, R. E.; Whitehead, K.; Assefa, Z. *Inorg. Chem.* **2008**, *47*, 1895−1897.
(42) Thomas, R. B.; Smith, P. A.; Jaleel, A.; Vogel, P.; Crawford, C.; Assefa, Z.; Sykora, R. E. *Inorg. Chem.* **2012**, *51*, 3399−3408.
(43) Stojanovic, M.; Robinson, N. J.; Chen, X.; Sykora, R. E. *Inorg. Chim. Acta* **2011**, *370*, 513−518.
(44) *Xcalibur CCD system, CrysAlisPro Software system*, Version 1.171.35; Oxford Diffraction Ltd.: Abingdon, U.K., 2012.
(45) Sheldrick, G. M. *Acta Crystallogr.* **2008**, *A64*, 112−122.
(46) Maynard, B. A.; Smith, P. A.; Jaleel, A.; Ladner, L.; Sykora, R. E. *J. Chem. Crystallogr.* **2010**, *40*, 616−623.
(47) Shannon, R. D.; Prewitt, C. T. *Acta Crystallogr., Sect. A* **1976**, *A32* (5), 751−67.
(48) Xia, B.-H.; Zhang, H.-X.; Che, C.-M.; Leung, K.-H.; Phillips, D. L.; Zhu, N.; Zhou, Z.-Y. *J. Am. Chem. Soc.* **2003**, *125*, 10362−10374.
(49) Loosli, A.; Wermuth, M.; Güdel, H.-U.; Capelli, S.; Hauser, J.; Bürgi, H. B. *Inorg. Chem.* **2000**, *39*, 2289−2293.
(50) Maffly, R. L.; Johnson, P. L.; Williams, J. M. *Acta Crystallogr., Sect. B* **1977**, *B33* (3), 884−887.
(51) Fukuda, Y.; Nakao, A.; Hayashi, K. *J. Chem. Soc., Dalton Trans.* **2002**, 527−533.
(52) Zhou, Z.-Y.; Liu, W.-N.; Liu, F.-F.; Fan, X.-J.; Zhan, X.-L.; Zhuang, L.-D.; Ma, G.-Z.; Cai, Y.-P. *Inorg. Chem. Commun.* **2010**, *13*, 1580−1584.
(53) (a) Colis, J. C. F.; Larochelle, C.; Staples, R.; Herbst-Irmer, R.; Patterson, H. *Dalton Trans.* **2005**, 675−679. (b) Assefa, Z.; Shankle, G.; Patterson, H. H.; Reynolds, R. *Inorg. Chem.* **1994**, *33*, 2187−2195. (c) Tanner, P. A.; Zhou, X.; Wong, W.-T.; Kratzer, C.; Yersin, H. *J. Phys. Chem. B* **2005**, *109*, 13083−13090. (d) Rawashdeh-Omary, M. A.; Larochelle, C. L.; Patterson, H. H. *Inorg. Chem.* **2000**, *39*, 4527−4534. (e) Assefa, Z.; DeStefano, F.; Garepapaghi, M. A.; LaCasce, J. H., Jr.; Ouellete, S.; Corson, M. R.; Nagle, J. K.; Patterson, H. H. *Inorg. Chem.* **1991**, *30*, 2868−2876.
(54) Werts, M. H. V.; Jukes, R. T. F.; Verhoeven, J. W. *Phys. Chem. Chem. Phys.* **2002**, *4*, 1542−1548.
(55) Beeby, A.; Bushby, L. M.; Maffeo, D.; Williams, J. A. G. *J. Chem.Soc., Perkin Trans. 2* **2000**, 1281−1283.
(56) Beeby, A.; Bushby, L. M.; Maffeo, D.; Williams, J. A. G. *J. Chem. Soc., Dalton Trans.* **2002**, 48−54.
(57) (a) de Sá, G. F.; Malta, O. L.; de Mello Donegá, C.; Simas, A. M.; Longo, R. L.; Santa-Cruz, P. A.; da Silva, E. F., Jr. *Coord. Chem. Rev.* **2000**, *196*, 165−195. (b) Moore, E. G. *Dalton Trans.* **2012**, *41*, 5272−5279.